Development and benchmark of a new analysis method dedicated to transverse beam emittance measurement

S. Morard, J. Michaud, E. Minaya Ramirez, L. Perrot

Development and benchmark of a new analysis method dedicated to transverse beam emittance measurement

S. Morard[a], J. Michaud[a], E. Minaya Ramirez[a], L. Perrot[a]

[a] *CNRS / IN2P3, IJCLab - Université Paris-Saclay, Orsay, 91400, France*

Abstract

A recent emittance measurement analysis pointed out the scarce calculation tools to evaluate precisely the method and error calculations. In this paper, a new analysis technique is proposed and compared on realistic beam simulations with the already existing linear regression method. This new analysis method is shown to be easier to implement and provides results with a good level of confidence. Detailed calculations of the errors obtained with an Allison scanner, as well as studies of the errors due to the analysis method, are presented.

Introduction

In a system subjected to linear forces, the particles occupy an elliptical space. Under non linear forces such as space-charge effects or fringe fields for example, the elliptical shape of the beam phase space can be deformed [1]. The transverse emittance of a beam is the region occupied by its particles in the phase space (x, p_x) or (y, p_y), where x and y are the position in the horizontal or vertical planes and p_x and p_y their associated momentum. The emittance ϵ is in fact defined by the mean particles' action J of the phase space.

$$\epsilon = 2\pi J \tag{1}$$

However position momemtum cannot be measured. To ensure physical meaning and obtain a measurable quantity, the emittance is redefined in the phase spaces (x, x') and (y, y'), with $x' = \frac{dx}{dz}$ and $y' = \frac{dy}{dz}$ the position angles, z being the trajectory axis of the beam. For a measurement, the transverse emittance becomes a statistical quantity, mathematically well defined by its expression presented in equation 2. All expressions valid for the phase space (x, x') are also valid for (y, y').

$$\epsilon_{rms} = \sqrt{\sigma_x^2 \sigma_{x'}^2 - \sigma_{xx'}^2} \tag{2}$$

with :

$$\sigma_x = \sqrt{< x^2 > - < x >^2} = \sqrt{\epsilon_{rms}\beta} \tag{3}$$

$$\sigma_{x'} = \sqrt{< x'^2 > - < x' >^2} = \sqrt{\epsilon_{rms}\gamma} \tag{4}$$

$$\sigma_{xx'} = \sum_i^N \frac{1}{N}(x_i - < x >)(x_i' - < x' >) = -\epsilon_{rms}\alpha \tag{5}$$

N is the total number of particles and $i \in [1, N]$. The parameters α, β and γ are the Twiss parameters, which give information on the size and orientation of the beam ellipse in its phase space. With the knowledge of the emittance, they are keys parameters to characterise a beam and be able to study transport, optical aberrations or other applications [1]. For these reasons, emittance measurements are performed in many accelerator facilities at low or high energy beams. The real value of the beam emittance is considered to be the measurable quantity ϵ_{rms} as defined by equation 2 which remains valid regardless of the particle distribution. Different types of techniques or detectors have been developed to succeed at evaluating the beam emittance. One of these is the three gradients method, using transfer matrix of quadrupoles and drift [2]. By using three different quadrupole strengths and measuring the beam size σ_x on a beam monitor, it is possible to extract the three differents parameters of the beam matrix defined in equation 6.

$$\begin{pmatrix} \sigma_x^2 & \sigma_{xx'} \\ \sigma_{xx'} & \sigma_{x'}^2 \end{pmatrix} = \epsilon_{rms} \begin{pmatrix} \beta & -\alpha \\ -\alpha & \gamma \end{pmatrix} \tag{6}$$

Using the same idea, employing three profile monitors could be used instead of varying three times a quadrupole strength. Dedicated beam diagnostics also have been developed for beam emittance measurements

Email address: morard@ijclab.in2p3.fr (S. Morard)

such as the pepper-pot emittancemeter and the Allison scanner [3, 4]. The first one is able to perform 4D transverse beam emittance measurements when the second one only performs 2D transverse measurements. 4D measurements are an advantage if both planes (x, x') and (y, y') are coupled. If not, separate 2D measurements of each plane are sufficient for a complete characterisation of the beam. The Allison scanner will be detailed in the next section. In the case of the pepper-pot emittancemeter, the beam particles pass through a collimator, which is a plate with small holes of same size located at same distance from each other so that the beam divergence can be deduced. The beam is then divided in beamlets by the holes and they propagate up to a detector within a known distance. The detector is in principle a microchannel plate (MCP) coupled to a CCD camera and a phosphorus screen. The pixels observed with the camera or the intensity measured with the MCP allow a reconstruction of the phase space of the beam. From the phase space obtained with an emittancemeter, the analysis is not straightforward and beam parameters are not easily extracted since background noise is involved during the measurement.

A question arose when an Allison scanner was used to perform emittance measurements as close as possible to the exit of the source at 30 kV at the research platform ALTO [5]. The detailed results of the measurements performed at ALTO will be published in a following article. However, during the measurement campaign, conservation of the beam emittance was not observed. Different values of the emittance were measured when various quadrupole strengths were applied. According to Liouville's theorem, in a Hamiltonian system, the volume occupied by all the particles in the phase space is conserved over the time evolution of the system. In the case of the rms emittance, which is sensitive to distortions of the particle distribution, its conservation remains true if the forces present are purely linear and respect Hamiltonian dynamics. In the case of ALTO, however, conservation of the rms emittance was not verified. Since the beam is only subjected to the electrostatic forces of the quadrupoles during the measurement, it was hypothesized that the beam's shape might bias the analysis. If the beam is very large such as illustrated in Figure 1 (a), the obtained value of emittance with the linear regression used in the literature is bigger than the value given for a smaller beam such as Figure 1 (b) [3].

It was decided to investigate more closely the analysis method used to obtain the emittance value and to estimate its associated error. This is the main purpose of the present article. After recalling the definition of emittance and Twiss parameters, as well as the possible devices or methods for measuring transverse beam emittance, we will take a closer look at the operation of the Allison scanner. Then, we will compare two methods of emittance analysis using particle distribution simulations: the first being the linear regression method found in the literature, and the second being the new method proposed. Finally, we will present the limitations of the proposed method.

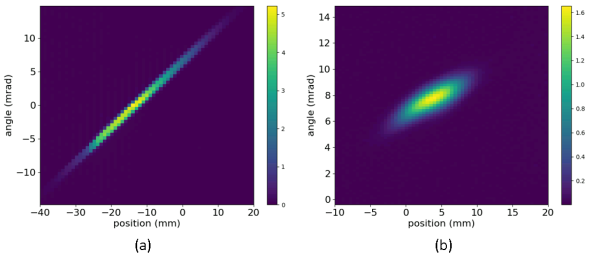

Figure 1: Example of two measurement with very different values of emittance when the only parameter changing is the strength of the quadrupoles.

1. Allison scanner

The description of this type of detector is based on the Allison scanner built at CNRS/IPHC-Strasbourg laboratory but the general principle remains the same [4, 6]. This Allison scanner was designed to measure low-energy ion beams.

1.1. Hardware

The IPHC Allison scanner has a movable probe with a thin aperture of $a = 0.075$ mm, controlled by a servo-motor, in order to obtain a beamlet at a given position. The range of the servo-motor limits the range of possible positions to measure. Inside the probe, two plates of variable and opposite potential, as shown in Figure 2, will deflect the incoming particles of the beamlet. A Faraday cup placed just after the rear slits measures the current induced by the particles passing as a function of applied voltage. The applied voltage differences between the two plates ΔV make it possible to obtain the angular distribution of the beam by equation 7 [6]. U is the kinetic energy of the particles and the other variables are distances represented in Figure 2.

$$x' = \frac{\Delta V}{4Ug} \frac{L_{eff} + 2\delta_2}{\delta_1 + \delta_2 + L_{eff}} \tag{7}$$

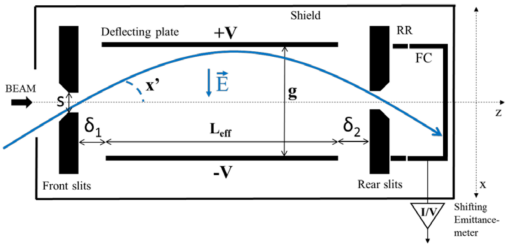

Figure 2: Allison scanner schematic view. A possible curved trajectory of a particle is shown in blue. The beam axis is in the z direction. *RR* : electron repeller, *FC* : Faraday cup

The design of the probe allows the access to the position and angular distributions of the beam, and each couple (x, x') has an associated measured intensity I. This applies not only to the IPHC's emittancemeter but to all Allison scanners.

1.2. Electronics

The deflecting plate potential of the IPHC Allison scanner is obtained with a ± 700 V DC bipolar power amplifier. The range of polarization gives a limitation on the possible divergence measurement of the beam. An electron repeller of -1000 V is also coupled to the Faraday cup to ensure that only the desired ions are measured. The beam particles induce a current on the Faraday cup, and the electronic signal undergoes transformation. The signal first passes through a current/voltage converter [7]. With this element, an offset can be controlled before the conversion and an amplification of the voltage signal is possible by applying a gain up to 10^{11}. Finally the signal goes through an Analog to Digital Converter coding on 16-bits. The numerical signal is then exploited using a control system based on LabVIEW [8]. In general cases, the polarization ranges of the plates or the accuracy of the electrical devices will depend on the emittance range to be measured and the desired accuracy of the emittancemeter.

1.3. Software and control

Allison scanners require to monitor various parameters, including the scanning range in position, divergence, and measurement duration. The LabVIEW interface allows users to control these parameters but also to display the acquisition progress during a measurement, as shown in Figure 3. One key adjustable parameter is the measurement step, which users can set within the limits defined by the servo-motor for position and the power supplies for angle. It will affect the precision and the time of the measurement. Other significant parameters, not shown on Figure 3, are the HT-wait and the orientation of the emittancemeter. The HT-wait defines a time to wait after applying a voltage on the deflection plates and before the start of the signal recording. Sufficient time is required for the electronic stabilisation in order to not affect the angle measurement by amplifying the background noise. Defining the correct orientation of the Allison scanner on the beam line is important in order to have the appropriate x and x' axis during a measurement. One final major parameter that the user needs to define is the reference position to determine the beam center.

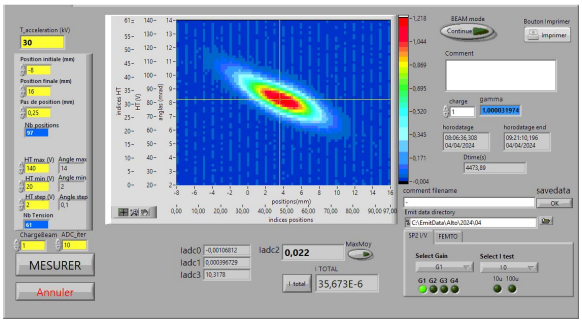

Figure 3: LabVIEW panel with an example of an emittance measurement with some of its parameters. The yellow area on the left indicates the parameters accessible to the user (beam energy, position, voltage steps). The right part of the figure gives information on the location of the saved files and the time of the measurement.

The data from a measurement are saved to file in the ASCII format presented in Figure 4. The file header summarizes the measurement steps, including the minimum and maximum limits and the number of measurement points for both position and angle, along with the beam energy. Each position and angle are associated to an index value. At the end of measurement, the (x, x') data of the 2D histogram are written in columns. The first column is the time index, which is not used, the second and third columns give the position and angle indices and the fourth column represents the measured intensity.

```
fichier  emittance: X
HT ion (kV) : 30.000000
frequence (Hz) : 1
N points temps : 1
pas de position (mm) : 2.000000
N points  position (mm) : 45
N points angle (mrad) : 283
vecteur positions (mm) : 28.000000 26.000000 24.000000 22.000000 20.000000 18.000(
vecteur angles (mrad) : 69.709316 69.214923 68.720531 68.226139 67.731746 67.2373
type d'ion : ..............
colonnes de 1 a 4 : indice de temps / indice position / indice angle / I [Volt] :
0.0     0       0       0.015689
0.0     0       1       0.010049
0.0     0       2       0.010107
0.0     0       3       0.009671
0.0     0       4       0.009061
0.0     0       5       0.008994
0.0     0       6       0.007849
0.0     0       7       0.008865
```

Figure 4: Example of ASCII file produced after an emittance measurement.

1.4. Calculation of emittance error due to Allison scanner

Error calculations for beam emittance measurements obtained in the form of a 2D histogram have already been developed. However, these calculations were performed under the assumption of a centered beam, which uses simplified expressions of equations 3 and 4 [9]. The following demonstration uses the most general expressions, presented in equations 3 and 4. This means that the calculations can be used for any emittance measurement where data on position x, angle x' and an intensity I are recorded. As a reminder, all expressions valid for the (x, x') plane are also true for the (y, y') plane.

With data from an Allison scanner, equations 3 to 5 cannot be directly applied since no information on the number of particles per couple (x, x') is available, only the intensity I is measured and transformed into a voltage. Therefore, these equations need to be adapted. Using the weighted average $w(x)$ defined in equation 8, new expressions for σ_x, $\sigma_{x'}$ and $\sigma_{xx'}$ are obtained in equation 9 to 11.

$$w(x) = \frac{\sum_i x_i I_i}{\sum_i I_i} \tag{8}$$

$$\sigma_x = \sqrt{w(x^2) - w(x)^2} \tag{9}$$

$$\sigma_{x'} = \sqrt{w(x'^2) - w(x')^2} \tag{10}$$

$$\sigma_{xx'} = w([x - w(x)][x' - w(x')]) \tag{11}$$

In general, for a function f with two variables a and b with known associated errors δa and δb, error δf is calculated by the equation 12 [10].

$$\delta f(a,b) = \sqrt{\left(\frac{\partial f}{\partial a}\right)^2 \delta a^2 + \left(\frac{\partial f}{\partial b}\right)^2 \delta b^2} \tag{12}$$

Equation 2 and equations 8 to 11 depend on x, x' and I whose errors δx, $\delta x'$ and δI are known. The following equation can be thus obtained for the weighted average:.

$$\delta w(x) = \sqrt{\sum_i \left(\frac{\partial w(x)}{\partial x_i}\right)^2 \delta x^2 + \sum_i \left(\frac{\partial w(x)}{\partial I_i}\right)^2 \delta I^2} \tag{13}$$

with

$$\frac{\partial w(x)}{\partial x_i} = \frac{I_i}{\sum_i I_i} \tag{14}$$

and

$$\forall k \in [1, N], \frac{\partial w(x)}{\partial I_i} = \sum_{k \neq i} \frac{(x_i - x_k) I_k}{\left(\sum_i I_i\right)^2} \tag{15}$$

The sums are calculated over all position and divergence pairs. Errors δx, $\delta x'$ and δI are directly linked to the conception of the Allison scanner and associated electronics chain up to the ADC. The motor precision and the aperture size of the probe will set the value of δx. The aperture size also has an impact on $\delta x'$ as does the precision of the power supply to the plates curving the trajectory of particles inside the probe [4]. The precision of the ADC will give the error for δI.

Knowing the expression for the error of the weighted mean, we can then calculate the error for σ_x and σ'_x.

$$\delta\sigma_x = \sqrt{\left(\frac{1}{2\sigma_x}\right)^2 \delta w^2(x^2) + \left(\frac{w(x)}{\sigma_x}\right)^2 \delta w^2(x)} \tag{16}$$

where

$$\delta w(x^2) = \sqrt{\sum_i \left(\frac{\partial w(x^2)}{\partial x_i}\right)^2 \delta x^2 + \sum_i \left(\frac{\partial w(x^2)}{\partial I_i}\right)^2 \delta I^2} \tag{17}$$

with

$$\frac{\partial w(x^2)}{\partial x_i} = \frac{2 x_i I_i}{\sum_i I_i} \tag{18}$$

and

$$\frac{\partial w(x^2)}{\partial I_i} = \sum_{k \neq i} \frac{(x_i^2 - x_k^2) I_k}{\left(\sum_i I_i\right)^2} \tag{19}$$

For $\delta\sigma_{x'}$, x can be replaced by x' in the above equations. The error $\delta\sigma_{xx'}$ is calculated in the following way :

$$\delta\sigma_{xx'} = \sqrt{D_x \delta x^2 + D_{x'} \delta x'^2 + D_I \delta I^2} \tag{20}$$

with

$$D_x = \sum_i \left(\frac{\partial \sigma_{xx'}}{\partial x_i}\right)^2 \tag{21}$$

$$D_{x'} = \sum_i \left(\frac{\partial \sigma_{xx'}}{\partial x'_i}\right)^2 \tag{22}$$

$$D_I = \sum_i \left(\frac{\partial \sigma_{xx'}}{\partial I_i}\right)^2 \tag{23}$$

where

$$\frac{\partial \sigma_{xx'}}{\partial x_i} = \frac{I_i}{\sum_i I_i}(x'_i - w(x')) - I_i \sum_k \frac{I_k}{\left(\sum_i I_i\right)^2}(x'_k - w(x')) \tag{24}$$

and

$$\frac{\partial \sigma_{xx'}}{\partial x'_i} = \frac{I_i}{\sum_i I_i}(x_i - w(x)) - I_i \sum_k \frac{I_k}{\left(\sum_i I_i\right)^2}(x_k - w(x)) \tag{25}$$

then

$$\begin{aligned}\frac{\partial \sigma_{xx'}}{\partial I_i} =& \frac{[x_i - w(x)][x'_i - w(x')]}{\sum_i I_i} \\ &- \frac{1}{\left(\sum_i I_i\right)^2} \sum_k I_k (x_k - w(x))(x'_k - w(x')) \\ &- \sum_{k \neq i} \frac{(x_i - x_k) I_k}{\left(\sum_i I_i\right)^3} \sum_j I_j (x'_j - w(x')) \\ &- \sum_{k \neq i} \frac{(x'_i - x'_k) I_k}{\left(\sum_i I_i\right)^3} \sum_j I_j (x_j - w(x))\end{aligned} \tag{26}$$

Finally, by applying equation 12 for evaluating the general emittance error due to the Allison scanner $\delta\epsilon_A$, the following expression is obtained :

$$\delta\epsilon_A = \sqrt{\left(\frac{\sigma_x \sigma_{x'}^2}{\epsilon}\right)^2 \delta\sigma_x^2 + \left(\frac{\sigma_{x'} \sigma_x^2}{\epsilon}\right)^2 \delta\sigma_{x'}^2 + \left(\frac{\sigma_{xx'}}{\epsilon}\right)^2 \delta\sigma_{xx'}^2} \tag{27}$$

This error can be propagated to additionally obtain the error on the Twiss parameters.

$$\begin{aligned}\delta\beta_A &= \sqrt{\left(\frac{\partial \beta}{\partial \sigma_x}\right)^2 \delta\sigma_x^2 + \left(\frac{\partial \beta}{\partial \epsilon_{rms}}\right)^2 \delta\epsilon_A^2} \\ &= \sqrt{\left(\frac{2\sigma_x}{\epsilon_{rms}}\right)^2 \delta\sigma_x^2 + \left(\frac{\sigma_x^2}{\epsilon_{rms}^2}\right)^2 \delta\epsilon_{rms}^2}\end{aligned} \tag{28}$$

$$\begin{aligned}\delta\alpha_A &= \sqrt{\left(\frac{\partial \alpha}{\partial \sigma_{xx'}}\right)^2 \delta\sigma_{xx'}^2 + \left(\frac{\partial \alpha}{\partial \epsilon_{rms}}\right)^2 \delta\epsilon_A^2} \\ &= \sqrt{\left(\frac{1}{\epsilon_{rms}}\right)^2 \delta\sigma_{xx'}^2 + \left(\frac{\sigma_{xx'}}{\epsilon_{rms}^2}\right)^2 \delta\epsilon_A^2}\end{aligned} \tag{29}$$

$$\begin{aligned}\delta\gamma_A &= \sqrt{\left(\frac{\partial \gamma}{\partial \sigma_{x'}}\right)^2 \delta\sigma_{x'}^2 + \left(\frac{\partial \gamma}{\partial \epsilon_{rms}}\right)^2 \delta\epsilon_A^2} \\ &= \sqrt{\left(\frac{2\sigma_{x'}}{\epsilon_{rms}}\right)^2 \delta\sigma_{x'}^2 + \left(\frac{\sigma_{x'}^2}{\epsilon_{rms}^2}\right)^2 \delta\epsilon_A^2}\end{aligned} \tag{30}$$

The errors introduced by the analysis method are also required to fully assess the error on the emittance value and the quality of the measurement. This will be covered in a following section.

2. Analysis method

In the literature there are several ways to exploit the data obtained with an Allison scanner [3, 11, 12, 13, 14, 15, 16, 17]. All techniques have in common the use of equation 2, but the difficulty lies in dissociating the background noise from the true beam signal. The question is then how to eliminate the noise with minimum contribution on the beam signal and without distorting the result of the emittance analysis, or how to evaluate the corresponding error $\delta\epsilon$ correctly. One way is to apply a threshold on the measured signal [11]. The majority of publications do not detail on how the emittance value is obtained [12]. There are also more sophisticated methods that have been developed such as a superposition of gaussian fit and/or elliptical fits [13] or a linear regression on the value of emittance as a function of the threshold applied on the signal [3, 13, 14]. However, these methods often lack sufficient information for reproducibility, may not report errors associated with the final result [15], or do not provide enough explanation on the results [16]. Additionally, none of these methods attempt to evaluate the Twiss parameters [17], which are crucial since the emittance alone does not fully characterise a beam.

In this section, we will study in more details the method using a linear fit which is the most commonly used at the moment based on previous references. We will also propose a new method. Both techniques will be compared with simulated particle distributions in order to find the best solution for our purpose.

2.1. Linear regression method

This method is based on gradually removing a portion of the signal and calculating the emittance for each threshold. The threshold n is a percentage of the maximum measured intensity I_{max}. The new intensity for all couples (x, x') is calculated with equation 31. We define I_{mes} as the initial measured signal with no threshold applied and I_{max} is the maximum value of all the values of I_{mes} for each couple (x, x'). The value I_{max} is never modified in the subsequent steps

$$I_j = I_{mes} - \frac{n}{100} I_{max} \tag{31}$$

with $n \in [0; 100]$ and $j \in [1, N_{bin}]$, where N_{bin} is the number of bins of the 2D histogram. Before using I_j for the calculation of emittance and its associated error, values I_j are normalised between $[0, 1]$ such as $\sum_1^{N_{bin}} I_j = 1$. After each subtraction, negative values are all set to 0 as to not to bias calculations. Since there was no real explanation as to when to stop the subtraction procedure in the previous references, it was decided to stop when $\epsilon_{rms} - \delta\epsilon_A \leq 0$ because a null or negative emittance has no physical meaning. The characteristic plot of emittance as a function of n obtained with this method is presented in Figure 5. It is observed that after a sharp decrease of the value of

emittance for the first few percent, due to the removal of background noise, the emittance decreases more slowly and with a linear tendency. This abrupt change of slope doesn't necessarily happen in the first few percent, it depends on the signal-to-noise ratio. In the exemple of Figure 5, the signal-to-noise ratio was very good. The

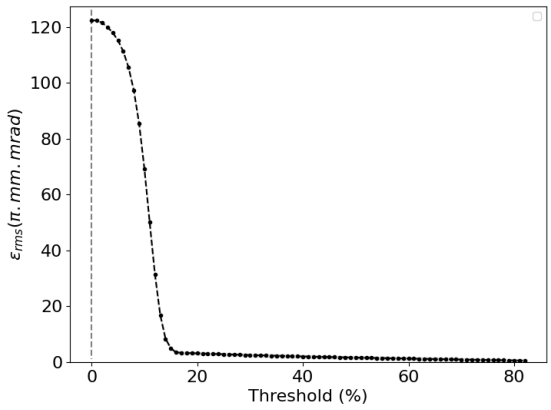

Figure 5: Example of calculated emittance as function of the number of removed percent of I_{max} for an emittance scan with an Allison emittancemeter.

hypothesis of this method is that if a linear regression is applied to the linear trend and extrapolated to zero, then $\epsilon_{rms} = \epsilon_{rms}(0)$. At zero, since no bias is introduced to the signal due to the analysis, $\epsilon_{rms}(0)$ represent the true value free from background noise.

A new question arises if a zoom is applied to the plot of Figure 5, which is shown in Figure 6. Where should the linear regression start ? Since there is no real answer in the literature, it was decided to look for the maximum slopes in the upper and lower areas defined by the emittance errors. To achieve this, linear regressions were initiated from the last calculated emittance value, $\epsilon_{rms}(n)$. Points are added one by one. If the line exceeds the error margin defined by $\epsilon_{rms}(n) \pm \delta\epsilon_A(n)$, the point is rejected, and the previous point is designated as the starting point for the regression. Both the minimum and maximum error limits are tested to obtain the minimum and maximum regressions shown on Figure 6 as yellow and red straight lines.

To obtain the parameters of the linear regression $f(x) = ax + b$ which takes into account the errors calculated for each value of emittance, the function *curve_fit()* from the *scipy* library of Python is used [18, 19]. Finally, the result is $\epsilon_{rms} = b \pm \delta b$, where b and δb are directly given by the function *curve_fit()*.

Another difficulty arises when in some cases, another

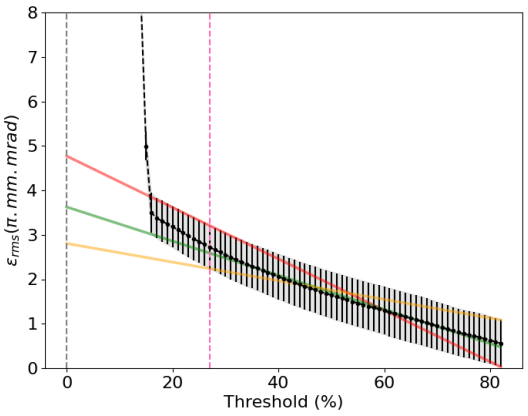

Figure 6: Zoom of Figure 5 in the vertical coordinate with additional linear regression.The red line represents the maximum slope that ends at the last point minus its error. The yellow line is the maximum slope that ends at the last point plus its error. The green line is the linear regression between the last and and start points given by the red and yellow lines. The grey are is the region of emittance values within the errors. The pink dotted line shows the starting point of the linear regression defined by the maximum and minimum linear regression.

sharp change of slope was observed for very high threshold values. This is because too much signal was removed and very few values of I_j are not equal to 0. It is unclear whether an emittance can still be accurately assessed with so few data points. Consequently, it has been decided to stop the regression earlier. This will be illustrated in subsection 2.3. In addition to the first stopping condition $\epsilon_{rms} \pm \delta\epsilon_A \leq 0$, a condition on the fluctuation of the slope is added. For this, the first derivative of ϵ_{rms}, σ_x, $\sigma_{x'}$ and $\sigma_{xx'}$ as a function of the threshold is calculated. In Figure 7, we can observe that after the red dotted line, which marks the stopping point, all the derivatives begin to fluctuate more significantly than before the red line. These fluctuations suggest that the last few signal points must be rejected from the linear regression. Starting from the initial point of the linear regression, an average of the derivatives of σ_x, $\sigma_{x'}$ and $\sigma_{xx'}$ are calculated and updated with each new point added. These averages are noted respectively $\overline{D_{\sigma_x}}$, $\overline{D_{\sigma_{x'}}}$ and $\overline{D_{\sigma_{xx'}}}$. Each derivative is compared to the average; if the value of two of the three derivatives is greater than the average by a factor 1.4, the corresponding point determines the last emittance value used for the linear regression. Different factors between 1 and 2 have been tested and the factor 1.4 is the one that gives the best results, indicating that the value of ϵ_{rms} is accurate within the margin of error $\delta\epsilon_A$, and corresponds to the smallest value of $\delta\epsilon_A$

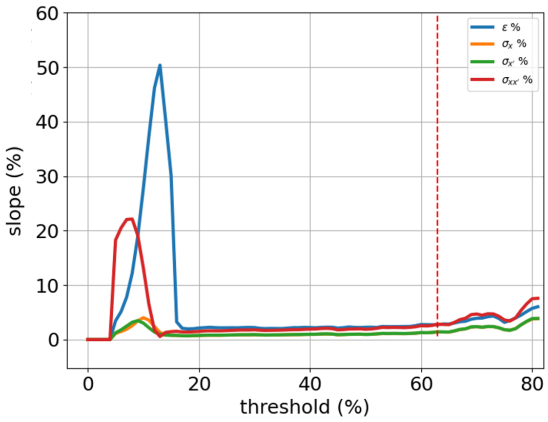

Figure 7: First derivative expressed in percent of ϵ_{rms}, σ_x, $\sigma_{x'}$ and $\sigma_{xx'}$ as a function of the threshold. The red dotted line shows the stopping point. Between 0 and 20, the large variation is due to the subtraction of a major part of the background noise.

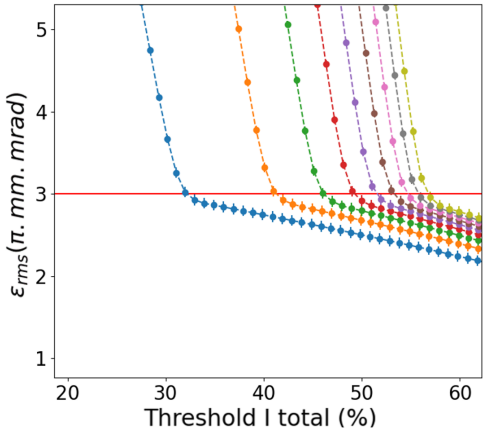

Figure 8: Calculated emittance as a function of threshold on I_{tot}. Each curve with a different color has a different signal-to-noise ratio ranging from 32 % to 57 %. The red line shows the real value of the emittance.

observed. It is not necessary to impose a condition on the derivative of the emittance, as it depends on the other three.

Finally, the exact same method of linear regression, with or without stopping condition, can be applied for σ_x, $\sigma_{x'}$ and $\sigma_{xx'}$ to extract the Twiss parameters.

2.2. *The proposed new method*

When applying a threshold on the total measured signal $I_{tot} = \sum_{j=1}^{N_{bin}} I_j$ and not on the maximum signal I_{max} and calculating the emittance, it was noticed that the sharp change of slope always happened at around the same value of emittance independently of the signal-to-noise ratio (3 π.mm.mrad in the exemple given in Figure 8). This was verified with different simulated distributions of particles where the emittance is precisely known. The intensity for the j-th bin of the 2D-histogram is calculated with equation 32. N_{bin} is the total number of bins not equal to 0. It changes each time a new threshold is applied, since the newly calculated values of I_j which fall below 0 are always set to 0, as previously done. The same method described in section 1.4 is applied to calculate the emittance and Twiss parameters and their associated error.

$$I_j = I_{mes} - I_{tot}\frac{n}{100N_{bin}} \tag{32}$$

The second derivative of the $\epsilon_{rms} = f(threshold)$ profile displayed in Figure 8 shows systematically a maximum for a given threshold depending on the background level (see fig. 9). For a same particle distribution, these maxima of $\epsilon_{rms} = f(threshold)$ occur systematically at the same emittance value (red line on fig. 8). The additional studies in this paper have been carried out based on this observation. Finding the maximum of the second derivative give the position of the threshold which correspond to the right value of the emittance and associated errors. The same methodology is used for the Twiss parameters.

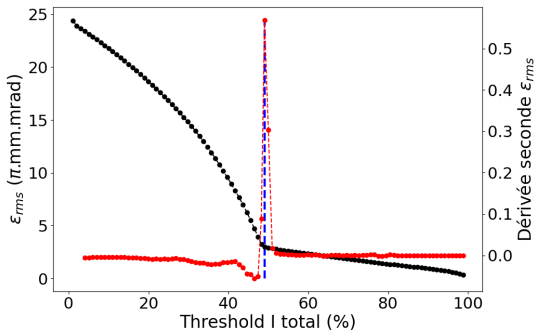

Figure 9: In red is represented the curve of the second derivative of the calculated emittance as a function of the threshold on I_{tot}, and the black curve correponds to the calculated emittance as a function of the threshold on I_{tot}. The blue dotted line shows the correspondance between the maximum of the second derivative and the real value of the emittance.

2.3. *Simulation and Comparison*

The two analysis methods are studied and tested using simulated particle distributions, for which the emit-

tance and Twiss parameters are known. Consequently, it is possible to evaluated the strength and limits of each method and determine the best technique to use on real data.

2.3.1. Generated particles distributions

To generate particle distributions, the TraceWin code developed by CEA IRFU is used [20]. Various particle distributions of different shape, size and emittance are generated with 10^9 particles uniformly filling the 4D hyper-ellipsoid in phase-space. Two of them were deformed to simulate higher order effects. Two examples are shown in Figure 10. All the relevant information on

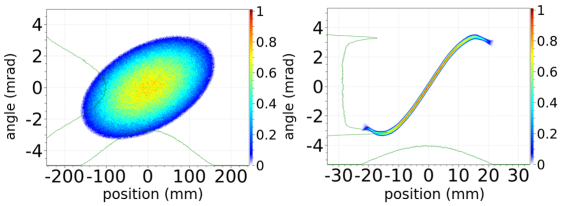

Figure 10: Exemples of generated distributions.

the generated distributions are listed in Table 1. These

Id	ϵ_{rms}	β	α	γ
1	1.0	2.0	-0.5	0.6
2	1.0	3.0	-7.0	16.7
3	1.0	5.0	-2.0	1.0
4	1.0	15.0	-15.0	15.0
5	3.0	5.0	-2.0	1.0
6	3.0	15.0	-15.0	15.0
7	3.0	50.0	-30.0	18.0
8	10.0	2.0	-0.5	0.6
9	10.0	5.0	-2.0	1.0
10	80.0	55.0	-0.5	0.0
11	4.2	4.7	-7.8	13.2
12	4.2	33.6	-4.9	1.2

Table 1: Emittance and Twiss parameters of the different generated distributions denoted by a number Id. Id 11 and 12 are distributions with higher-order effects.

distributions are then converted to histograms in order to reproduce the typical measured spectrum. To reproduce as much as possible the measurements done at the ALTO facility with the Allison scanner, a bin size of 0.5 mm in position and 0.3 mrad was chosen. The number of particles per bin I_{part_j}, where j corresponds to the bin number, is converted to an intensity value close to the one of a measured signal (see eq. 33). The factor b can be adjusted to modify the signal-to-noise ratio. It was set arbitrarily to 0.9 and remained unchanged while conducting the tests in this section. $Max(I_{part_j})$ corresponds to the maximal value of I_{part_j} in the histogram.

$$I_{part_j} = \frac{b \cdot I_{part_j}}{Max(I_{part_j})} \tag{33}$$

To simulate a measurement with an Allison scanner, it is also necessary to add a background noise I_{noise} to the histogram using equation 34. A gaussian background noise with $\mu = 0.02$ and $\sigma = 0.01$ was simulated with parameters taken from a background measurement with the Allison scanner.

$$I_{part_j} = I_{part_j} + I_{noise_j} \tag{34}$$

Following this last modification, the histogram is now as close as possible to a measurement and the different analysis methods can be applied. The linear regression has been tested with and without the stopping condition presented in subsection 2.1.

2.3.2. Results

Tables 2 and 3 present the compiled results obtained with the three different methods presented in subsection 2.1 and 2.2. Method 1 uses the linear regression with only $\epsilon_{rms} \pm \delta\epsilon_A \leq 0$ as a stopping condition. Method 2 is the same with the additional stopping condition on the average of the first derivative. Method 3 is based on using the maximum of the second derivative (new proposed technique). All emittance and Twiss parameters results are compiled in Table 2 and 3.

The most noticeable result is that if the distribution shape is very stretched (Ids 2, 4, 6, 7, 11 and 12), the errors are very large with the three methods. For Id 4, the results obtained with the linear regression are not even exploitable. Indeed, from Figure 11, it is observable that there are too few points to apply a correct linear regression. No reliable region where the emittance varies linearly with the threshold has been reached. In case of Id 1, 3 and 8, all three methods give satisfying results, though the value of the emittance is slightly overestimated with the linear regression methods. Another outcome of this study is that the linear regression method has more difficulties to evaluate the correct Twiss parameters (see Table 2 and 3). We can't use the error calculated on the emittance since the value is extrapolated. However, the errors of the Twiss parameters are directly linked to the emittance error. This is not the case when the second derivative method is used. Another difficulty is noticed with the linear regression in the cases of Id 9 and 10. There is more than one linear slope where the regression could be applied for a

Id		Method 1	Method 2	Method 3
1	ϵ_{rms}	1.2 ± 0.0	1.2 ± 0.0	1.0 ± 0.0
	β	2.6 ± 0.4	2.1 ± 0.1	2.0 ± 0.1
	α	−0.4 ± 0.0	−0.5 ± 0.0	−0.5 ± 0.0
	γ	0.6 ± 0.2	0.7 ± 0.1	0.6 ± 0.0
2	ϵ_{rms}	1.2 ± 0.7	1.2 ± 0.8	1.1 ± 0.4
	β	3.5 ± 0.6	3.4 ± 0.7	2.6 ± 0.8
	α	−6.6 ± 0.6	−6.6 ± 0.9	−6.1 ± 1.9
	γ	18.7 ± 2.1	18.5 ± 2.9	14.5 ± 4.3
3	ϵ_{rms}	1.1 ± 0.0	1.1 ± 0.2	1.0 ± 0.1
	β	6.1 ± 0.5	5.0 ± 0.7	4.9 ± 0.4
	α	−2.1 ± 0.0	−1.9 ± 0.2	−2.0 ± 0.1
	γ	1.2 ± 0.2	1.0 ± 0.4	1.0 ± 0.1
4	ϵ_{rms}	15.0 ± 6.3	20.3 ± 3.2	1.1 ± 0.7
	β	1.4 ± 0.3	1.2 ± 0.2	12.8 ± 6.2
	α	−1.0 ± 0.1	−0.8 ± 0.0	−12.8 ± 6.2
	γ	1.1 ± 0.3	1.0 ± 0.2	12.8 ± 6.2
5	ϵ_{rms}	3.4 ± 0.1	3.5 ± 0.1	3.0 ± 0.1
	β	5.7 ± 0.2	5.5 ± 0.2	4.9 ± 0.1
	α	−1.9 ± 0.0	−1.9 ± 0.0	−2.0 ± 0.0
	γ	1.1 ± 0.1	1.1 ± 0.1	1.0 ± 0.0
6	ϵ_{rms}	3.3 ± 5.9	3.3 ± 5.9	3.0 ± 1.0
	β	16.4 ± 1.3	16.1 ± 5.4	14.3 ± 4.6
	α	−14.7 ± 1.5	−14.5 ± 4.8	−14.4 ± 4.6
	γ	16.6 ± 1.9	16.3 ± 5.4	14.4 ± 4.6

Table 2: Emittance and Twiss parameters obtained for the different distributions presented in Table 1 from Id 1 to 6, using the methods presented in section 2.1 and 2.2.

Id		Method 1	Method 2	Method 3
7	ϵ_{rms}	44.0 ± 18.1	44.4 ± 27.7	3.1 ± 2.8
	β	4.7 ± 0.6	4.7 ± 0.4	46.1 ± 20.7
	α	−2.4 ± 0.3	−2.4 ± 0.2	−27.6 ± 12.4
	γ	1.6 ± 0.2	1.6 ± 0.1	16.6 ± 7.5
8	ϵ_{rms}	8.9 ± 0.1	11.5 ± 0.2	10.0 ± 0.0
	β	3.8 ± 0.3	2.6 ± 0.1	2.0 ± 0.0
	α	−0.4 ± 0.0	−0.5 ± 0.0	−0.5 ± 0.0
	γ	0.6 ± 0.1	0.9 ± 0.0	0.6 ± 0.0
9	ϵ_{rms}	7.8 ± 0.3	7.5 ± 0.4	10.0 ± 0.1
	β	10.9 ± 0.5	11.3 ± 0.6	5.0 ± 0.0
	α	−2.1 ± 0.0	−2.3 ± 0.0	−2.0 ± 0.0
	γ	1.8 ± 0.2	1.7 ± 0.2	1.0 ± 0.0
10	ϵ_{rms}	65.1 ± 0.4	98.4 ± 0.7	79.7 ± 0.1
	β	83.3 ± 2.7	60.9 ± 2.7	54.6 ± 0.1
	α	−0.5 ± 0.0	−0.5 ± 0.0	−0.5 ± 0.0
	γ	0.0 ± 0.0	0.0 ± 0.0	0.0 ± 0.0
11	ϵ_{rms}	4.7 ± 3.9	4.1 ± 5.2	4.3 ± 0.7
	β	4.9 ± 0.4	5.4 ± 1.2	4.6 ± 0.8
	α	−7.6 ± 0.5	−8.4 ± 1.7	−7.6 ± 2.1
	γ	13.9 ± 1.1	15.4 ± 3.2	12.6 ± 2.1
12	ϵ_{rms}	9.2 ± 6.2	11.9 ± 5.5	3.7 ± 0.6
	β	14.9 ± 1.5	11.3 ± 1.3	22.6 ± 3.0
	α	−2.9 ± 0.3	−2.2 ± 0.2	−5.3 ± 0.7
	γ	0.7 ± 0.2	0.6 ± 0.1	1.3 ± 0.2

Table 3: Emittance and Twiss parameters obtained for the different distributions presented in Table 1 from Id 7 to 12, using the methods presented in section 2.1 and 2.2.

same distribution (see fig. 12). The emittance value can be overestimated, as seen on the left of Figure 12, or underestimated, as shown on the right. This demonstrates that neither slope is able to accurately evaluate the correct emittance value. This is not due to the simulated distribution, as this issue was also encountered with real measurements. Finally, one last result concerns the distributions with higher-order effects (Id 11 and 12). Id 12 has more deformation because of more higher-order effects [21]. Even though the new method succeeds in evaluating the beam parameters, it has difficulties to give a good estimation of the Twiss parameter β for Id 12, but it is also more difficult to draw an ellipse on very deformed beam.

To conclude, the new method is more efficient to evaluate both the emittance and the Twiss parameters. The errors are also more reliable, as they are directly derived from the calculations. The new proposed method is easier to implement and also faster. However, caution is required. These tests were conducted under good conditions, with appropriated binning, a correct signal-to-noise ratio below 40% and threshold steps of 1%. It is essential to investigate whether these parameters can influence the obtained beam parameters and to determine if additional sources of error need to be considered.

3. Evaluation of additional errors

In this section, the step contribution during a measurement, the threshold step and the signal-to-noise ratio set up in the previous section are all tested separately with the new proposed method. Each of them are supposed to be independent. If necessary they can be included with $\delta\epsilon_A$ to give the full error on the emittance $\delta\epsilon_{rms}$ in equation 35. $\delta\epsilon_{bin}$ represents the error introduced by the step contribution. $\delta\epsilon_t$ accounts for errors associated with the threshold step and $\delta\epsilon_{SN}$ reflects the error related to the signal-to-noise ratio.

$$\delta\epsilon_{rms} = \sqrt{\delta\epsilon_A^2 + \delta\epsilon_{bin}^2 + \delta\epsilon_t^2 + \delta\epsilon_{SN}^2} \qquad (35)$$

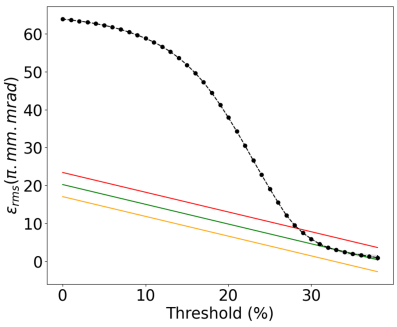

Figure 11: Emittance calculation as a function of applied threshold. The green line is the linear regression giving the value of emiitance using Method 2. The red and yellow lines are obtained with the linear regression applying plus or minus its error.

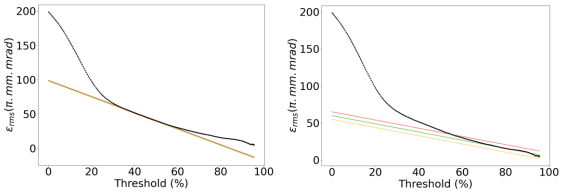

Figure 12: Emittance calculation as a function of the threshold applied with linear regression in case of Id 10. The left one was applied with stopping condition on the change of slope, and on the right without this stopping condition.

3.1. Measurement steps

The measurement duration with an Allison scanner is directly linked to the measurement step. It can be very long, up to a few hours, as the emittancemeter takes the same amount of time to measure each point. Therefore, the smaller the steps, the longer the measurement. Over time, experimental difficulties may arise, such as beam instability, which can affect the measurement. Users must always try to find the best compromise between the time and the precision of the measurement. It is very important to evaluate the impact of the step in position and divergence on the determination of the emittance and the Twiss parameters.

The influence of the measurement step is independent of the analysis method. To evaluate it, all distributions presented in section 2.3.1 are converted to many different histograms with bin_x length $\in [0.25; 5]$ mm and a $bin_{x'}$ length $\in [0.1; 3]$ mrad. In this instance, no simulated background noise is added so as to have no other contribution on the emittance calculation than the binning. After analyzing a distribution as a function of the binning in position and divergence, we can obtain a representation similar to what is shown in Figure 13. In all cases, it is immediately observed that the binning is size dependent. The smaller σ_x and $\sigma_{x'}$ are, the smaller the binning must be to have a precise evaluation of ϵ_{rms}. It is very difficult to evaluate $\delta\epsilon_{bin}$. It has been decided to define a region where the emittance error will be $\delta\epsilon_{bin} \leq 10\%$. In real measurement conditions, it is necessary to have an order of magnitude of the real beam size in order to set the good scanning settings. For this, a first quick measurement can be done and a fast evaluation of σ_x, $\sigma_{x'}$ and ϵ_{rms} is possible. From a complete analysis of the simulated distribution (see Table 1), empirical formulae are derived. These formulae estimate the upper limit of measurement steps in order to remain within the fluctuation area of 10% (see eq. 36 and 37).

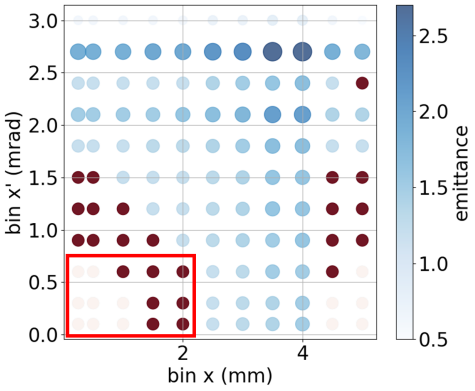

Figure 13: Example of emittance calculation in function of the binning in position and divergence for the case of Id 1 (see Table 1). The size and color of dots depends on the range of emittance value. Pink and grenat dots identify binning in position and divergence where the emittance does not exceed a 10% discrepancy from the theoretical emittance. The red rectangle shows the 10% fluctuation area, defined to ensure that the error cannot be increased.

$$bin_x = \frac{0.8 \cdot \epsilon_{rms_e}}{0.6 \cdot \sigma_{x'_e}} \tag{36}$$

$$bin_{x'} = \frac{1.4 \cdot \epsilon_{rms_e}}{2.0 \cdot \sigma_{x_e}} \tag{37}$$

ϵ_{rms_e}, $\sigma_{x'_e}$ and σ_{x_e} would be the parameters of the beam estimated with a quick first measurement. Respecting this, $\delta\epsilon_{bin} = 0.1\epsilon_{rms}$.

3.2. Threshold step

The threshold step determines the percentage of the total signal removed between each emittance evaluation within the same analysis. To test the robustness of the method, a step between 1 and 5% is studied to check if the maximum of the second derivative is shifting. From Figure 14, for very stretched distributions (Id 5 and 6),

it is observed that the threshold step doesn't have a noticeable impact since the error $\delta\epsilon_A$ due to the Allison scanner is already very large. However for bigger distributions (Id 8 and 10) where $\delta\epsilon_A$ becomes negligible, the threshold step effect is more visible. For every distribution (see Table 1), we can notice that a step of 1% is the best. But a larger step can widely improve the time calculation and a 5% step is not necessarily worse than a step of 2 or 3%. The threshold step doesn't induce a modification higher than 5% on the results of the emittance calculations. It can be considered that the error due to the threshold step is $\delta\epsilon_t \leq 5\%$. We can write $\delta\epsilon_t = 0.05 \cdot \epsilon_{rms}$.

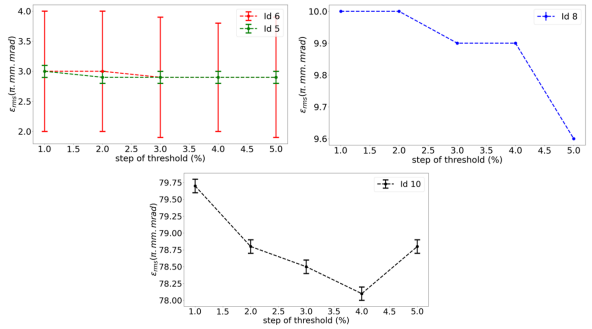

Figure 14: Emittance value and its associated error as a function of the threshold step for different phase-space distributions (see Table 1).

3.3. Signal-to-noise ratio

As shown in Figure 8, sharp change in slope appears when calculating the emittance as a function of the threshold on I_{tot}. In this case, the true emittance value lies within the range defined by the emittance value and its associated error bars, even when the signal-to-noise ratio is degraded. The goal here is to determine whether it is true for every threshold or if an additional error term $\delta\epsilon_{SN}$ is needed. Each distribution was tested by varying the value of $b = 0.9$ in equation 33. Figure 15 displays the results for beam distributions with very different characteristics. For very stretched distributions, the error $\delta\epsilon_A$ dominates every other error. In any other case, a very good signal-to-noise ratio allows the best evaluation of the emittance. The emittance estimation with this method is good enough for a threshold value corresponding to the maximum second derivative lower than 70-75% where $\delta\epsilon_{SN} \leq 10\%$. In the end, $\delta\epsilon_{SN} = 0.1\epsilon_{rms}$.

Finally, equation 38 presents the general expression of the error on the emittance. In this equation a measurement step small enough that can be evaluated with

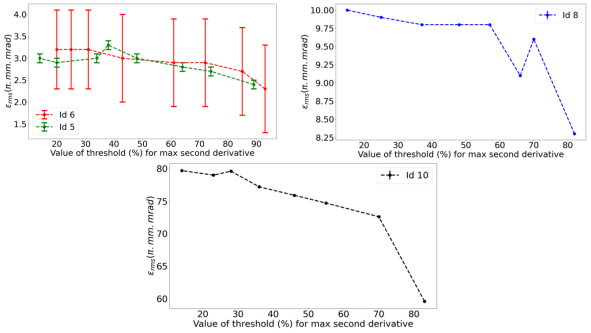

Figure 15: Emittance value and its associated error as a function of the threshold value corresponding to the maximum second derivative for different phase space distributions (see Table 1).

equations 36 and 37 is used. Threshold step has to be lower than 5%. The signal to noise ratio must not exceed the 75% threshold.

$$\delta\epsilon_{rms} = \sqrt{\delta\epsilon_A^2 + (0.1 \cdot \epsilon_{rms})^2 + (0.05 \cdot \epsilon_{rms})^2 + (0.1 \cdot \epsilon_{rms})^2} \tag{38}$$

The contribution of the error from the step measurement, the threshold step and the signal to noise ratio is the same for the Twiss parameters α, β and γ.

$$\delta\beta = \sqrt{\delta\beta_A^2 + (0.1 \cdot \beta)^2 + (0.05 \cdot \beta)^2 + (0.1 \cdot \beta)^2} \tag{39}$$

$$\delta\alpha = \sqrt{\delta\alpha_A^2 + (0.1 \cdot \alpha)^2 + (0.05 \cdot \alpha)^2 + (0.1 \cdot \alpha)^2} \tag{40}$$

$$\delta\gamma = \sqrt{\delta\gamma_A^2 + (0.1 \cdot \gamma)^2 + (0.05 \cdot \gamma)^2 + (0.1 \cdot \gamma)^2} \tag{41}$$

Conclusion

In this paper, we present a new analysis method to extract beam parameters with an Allison scanner. This new method was tested with known phase-space distributions. Using this method, we obtained the emittance and Twiss parameters for elliptical beams and beams with higher-order effects. Detailed calculations of the errors due to the Allison scanner were presented. We also added internal systematic errors due to the analysis method and measurement steps. This article provides all the tools to analyse similar data in other experiments. However, users must be careful with the quality of their measurement and adapt rigorously the possible errors. Finally, even if this method was developed for the analysis of an Allison scanner measurement, it can be used for any measurement that gives the information for reconstructing the phase space of a beam in a histogram,

such as a pepper-pot emittancemeter. The same methodology can be taken for the error calculation where only the value of δx, $\delta x'$ and δI have to be adapted for the instrument. An emittancemeter operates within a specific range of emittance due to its geometry and electronics. Therefore, it must be selected based on the expected order of magnitude.

References

[1] H. Wiedemann, *Particle Accelerator*, Fourth Edition, Springer, 2015.

[2] K. T. McDonald, D. P. Russell, *Methods of Emittance Measurement*, 1988.

[3] H. R. Kremers, J. P. M. Beijers, S. Brandenburg, *A pepper-pot emittance meter for low energy heavy-ion beams*, Rev. Sci. Instrum. 84, 025117, 2013.

[4] P. W. Allison et al, *An emittance scanner for intense low-energy ion beams*, IEEE Trans. Nucl. Sci., Vol. NS-30, No. 4, 1983.

[5] S. Essabaa et al, *The radioactive beam facility ALTO*, Nucl. Instrum. Meth. B, Vol. 317 218-222, 2013

[6] E. Bouquerel, C. Maazouzi, *IPHC Emittance-meters: Design and Development*, JINST 16 T06009, 2021.

[7] FEMTO, *Variable Gain High Speed Transimpedance Amplifier (Current Amplifier) DHPCA-100*, `https://www.femto.de/en/current-transimpedance-amplifier/dc-up-to-200-mhz-fast-variable-amplification-dhpca/`.

[8] B. Gergic and D. Hercog, *An Effective Concept for Teaching LabVIEW Programming to Engineering Students*, Appl. Sei. 20 24, 14(18), 8506.

[9] S. Jolly et al, *Data acquisition and error analysis for pepperpot emittance measurements*, Proceedings of DIPAC09, WEOA03, 421-423, 2009.

[10] P. R. Bevington, *Data reduction and error analysis for the physical sciences*, McGraw-Hill Higher Education, 2003.

[11] R. D'Arcy et al, *Distinct transverse emittance measurements of the PXIE LEBT*, Proceedings of IBIC2014, TUPD01, 393-397, 2014.

[12] M . P. Stockli et al, *Low-energy emittance studies with the new SNS allison emittance scanner*, Proceedings of PAC09, TH6REP012, 3974-3976, 2009.

[13] F. Osswald et al, *Transverse emittance measurement in 2D and 4D performed on a Low Energy Transport line : benchmarking and data analysis*, JINST 18 P01011, 2023.

[14] C. Richard et al, *Analysis of Allison scanner phase portraits using action-phase coordinates*, Proceedings of NAPAC2019, TUPLS08, 467-470, 2019.

[15] J. C. Wong, *High resolution phase space measurements with Allison-type emittance scanners*, Phys. Rev. Accel. Beam, 072801, 2019.

[16] T. Zhang et al. *High-level physics application for the emttance measurement by Allison scanner*, Proceedings of NAPAC2019, TUPLS05, 459-462, 2019.

[17] T. Gorlov et al., *Computation of space-phase effect in Allison scanner and its application to the measurement of emittance*, Proceedings of Hadron Beam, WGF06, 455-457, 2008.

[18] Python, Scipy library : `https://docs.scipy.org/doc/scipy/reference/generated/scipy.optimize.curve_fit.html`

[19] K. Vugrin et al. *Confidence region estimation techniques for nonlinear regression in groundwater flow: Three case studies.*, Water Resour. Res., Vol. 43, W03423.

[20] D. Uriot and N. Pichoff, *Status ofTRACEWIN code*, Proceedings of IPAC15, MOPWA008, 2015.

[21] C. K. Allen, T. P.Wangler *Beam halo definitions based upon moments of the particle distribution*, Phys. Rev. Accel. Beams, Volume 5, 2002.